AMERICAN SOCIETY FOR MICROBIOLOGY | Infection and Immunity®

BACTERIAL INFECTIONS

New Insights into the Role of Zinc Acquisition and Zinc Tolerance in Group A Streptococcal Infection

Cheryl-lynn Y. Ong,[a,b] Olga Berking,[a,b] Mark J. Walker,[a,b] Alastair G. McEwan[a,b]

[a]School of Chemistry and Molecular Biosciences, The University of Queensland, St. Lucia, Queensland, Australia
[b]Australian Infectious Diseases Research Centre, The University of Queensland, St. Lucia, Queensland, Australia

ABSTRACT Zinc plays an important role in host innate immune function. However, the innate immune system also utilizes zinc starvation ("nutritional immunity") to combat infections. Here, we investigate the role of zinc import and export in the protection of *Streptococcus pyogenes* (group A *Streptococcus*; GAS), a Gram-positive bacterial pathogen responsible for a wide spectrum of human diseases, against challenge from host innate immune defense. In order to determine the role of GAS zinc import and export during infection, we utilized zinc import (Δ*adcA* Δ*adcAII*) and export (Δ*czcD*) deletion mutants in competition with the wild type in both *in vitro* and *in vivo* virulence models. We demonstrate that nutritional immunity is deployed extracellularly, while zinc toxicity is utilized upon phagocytosis of GAS by neutrophils. We also show that lysosomes and azurophilic granules in neutrophils contain zinc stores for use against intracellular pathogens.

KEYWORDS zinc acquisition, zinc toxicity, nutritional immunity, group A *Streptococcus*, *Streptococcus pyogenes*, neutrophils

The acquisition of transition metal ions (zinc, manganese, and iron) by bacterial pathogens is recognized as being critical for their growth and survival. However, it has also been observed that elevated levels of metal can result in toxicity. Therefore, it is essential for bacteria to maintain tight control of metal ion homeostasis (1). Zinc is a significant component in the innate immune defense against bacterial pathogens (2). During an infection, nutritional immunity can occur, whereby the host withholds zinc from bacterial pathogens via redistribution of zinc by the Zn transporter (ZnT) and Zrt- and Irt-like protein (ZIP) families of proteins or zinc sequestration via calprotectin and metallothionein (3–7). *In vitro* studies have shown that zinc sequestration by calprotectin can inhibit the growth of various human pathogens, including *Staphylococcus aureus*, *Escherichia coli*, and *Enterobacter aerogenes* (5, 8, 9). On the other hand, elevated levels of zinc have been measured in different tissues of infected mice. Furthermore, zinc is observed to be released within macrophages and neutrophils subsequent to phagocytosis of bacterial pathogens (10–13). Unfavorable external conditions like excess extracellular zinc have been shown to exert toxic effects on bacterial cells by inhibiting manganese uptake and disrupting carbon metabolism (10, 14, 15). As a consequence, bacterial pathogens have evolved strict internal control of zinc homeostasis to combat fluctuating levels of extracellular zinc.

The human pathogen *Streptococcus pyogenes* (group A *Streptococcus* [GAS]) colonizes the skin and throat asymptomatically or causes mild superficial infections like impetigo and pharyngitis. Occasionally, GAS can penetrate into deeper tissues and may cause severe invasive diseases like septicemia, streptococcal toxic shock-like syndrome, and necrotizing fasciitis (16). GAS possesses well-defined systems for zinc efflux and uptake that ought to allow it to deal with fluctuating zinc concentrations. To efflux excess zinc, GAS possesses a cation diffusion facilitator, CzcD, that is regulated by a TetR family transcriptional regulator, GczA (11, 17). In order to import zinc, GAS possesses

Received 23 January 2018 **Returned for modification** 21 February 2018 **Accepted** 14 March 2018

Accepted manuscript posted online 26 March 2018

Citation Ong CY, Berking O, Walker MJ, McEwan AG. 2018. New insights into the role of zinc acquisition and zinc tolerance in group A streptococcal infection. Infect Immun 86:e00048-18. https://doi.org/10.1128/IAI.00048-18.

Editor Nancy E. Freitag, University of Illinois at Chicago

Address correspondence to Cheryl-lynn Y. Ong, y.ong@uq.edu.au.

M.J.W. and A.G.M. contributed equally to this work.

the ATP-binding cassette (ABC) transporter uptake system AdcABC, which is regulated by AdcR (9, 18, 19). As in *Streptococcus pneumoniae*, GAS encodes a second zinc-binding protein, AdcAII (also known as Lsp, Lmb, or Lbp) (19–21).

Previous study has shown that the deletion of *czcD* in GAS resulted in loss of virulence in both *in vitro* human neutrophil killing assays and subcutaneous invasive mouse virulence assays, indicating the importance of zinc export in pathogenesis (11). On the other hand, loss of zinc uptake has resulted in reduced ability to form lesions in the subcutaneous infection mouse model and reduced overall virulence in mice (9, 19). Furthermore, deletion mutations in the zinc import system have also resulted in reduced virulence in other streptococcal species (22–24). Additionally, forward genetic techniques like transposon mutagenesis and transposon sequencing (Tn-Seq) have shown that genes encoding the zinc import system, such as *adcA* and *adcC*, are important for growth in blood and fitness in the mouse (25, 26).

Although both zinc export and zinc import are established as having a role in the pathogenesis of GAS, information linking their relative roles in relation to the infection process is limited. To address this, we describe experiments in which the progress of infection in a murine model is compared for wild-type (WT) M1T1 GAS strain 5448, an isogenic Δ*czcD* deletion mutant (11), and a Δ*adcA* Δ*adcAII* double deletion mutant. Our findings indicate that zinc toxicity occurs primarily within innate immune cells, such as human neutrophils, whereas zinc starvation occurs extracellularly, possibly through a combination of different host responses, such as via the action of calprotectin. These results reveal the dynamic nature of metal intoxication/limitation in the context of the host-pathogen interaction.

RESULTS

Optimal zinc import in *Streptococcus pyogenes* requires both AdcA and AdcAII zinc-binding proteins. In order to investigate the role of zinc import in GAS fitness, we first set out to identify a suitable mutant that was highly compromised for zinc acquisition. The GAS M1T1 genome contains a number of genes involved in zinc import, including genes encoding a single ABC transporter, *adcB* (SP5448_00570; MGAS5005_Spy0077), *adcC* (SP5448_00560; MGAS5005_Spy0078), and two zinc solute-binding proteins (SBPs), *adcA* (SP5448_06840; MGAS5005_Spy0543) and *adcAII* (SP5448_08690; MGAS5005_Spy1711) (Fig. 1A) (9, 18). In the M1T1 GAS strain 5448, we observed that *adcA* expression was most downregulated (5-fold decrease) when grown under zinc overload conditions (Fig. 1B). *adc* gene expression is regulated by AdcR, which acts as a zinc-dependent repressor (18). Zinc overload induced *czcD* expression under these same conditions (Fig. 1B). Under zinc-limited conditions, *adcA* was over 20-fold upregulated, while *adcAII* was over 70-fold upregulated, indicating considerable induction of gene expression, which was mirrored by the repression of *czcD* expression (Fig. 1C). These results confirm tight control of the zinc homeostasis system in GAS and suggest that the combination of both AdcA and AdcAII is likely required for zinc import.

We next measured the effect of the deletion of different zinc homeostasis genes on GAS growth, using Δ*czcD*, Δ*adcA*, Δ*adcAII*, Δ*adcA* Δ*adcAII*, and Δ*adcBC* deletion mutants. In standard THY medium, all strains grew equivalently (Fig. 1D) and, as expected, only the *czcD* mutant was attenuated for growth in the presence of 1 mM zinc (Fig. 1E). In contrast, in the presence of the zinc chelator *N*,*N*,*N*′,*N*′-tetrakis(2-pyridylmethyl)ethylenediamine (TPEN), the growth of the *adcA*, *adcBC*, and *adcA adcAII* mutants was reduced (Fig. 1F) but the *adcAII* mutant was only modestly affected. In view of these observations, the *adcA adcAII* double mutant was chosen for comparison with the *czcD* mutant in subsequent experiments.

Effects of the loss of zinc import and zinc export systems on GAS virulence. In order to test the effect of genetic deletion of zinc import and zinc export systems, we infected transgenic human-plasminogenized mice subcutaneously with strain 5448 WT and the Δ*czcD* and Δ*adcA* Δ*adcAII* mutants. Mice infected with WT 5448 GAS developed skin lesions earlier than mice infected with either the Δ*czcD* or Δ*adcA* Δ*adcAII* mutant (Fig. 2A, 24 h). The lesion area was significantly larger in mice infected with 5448 WT

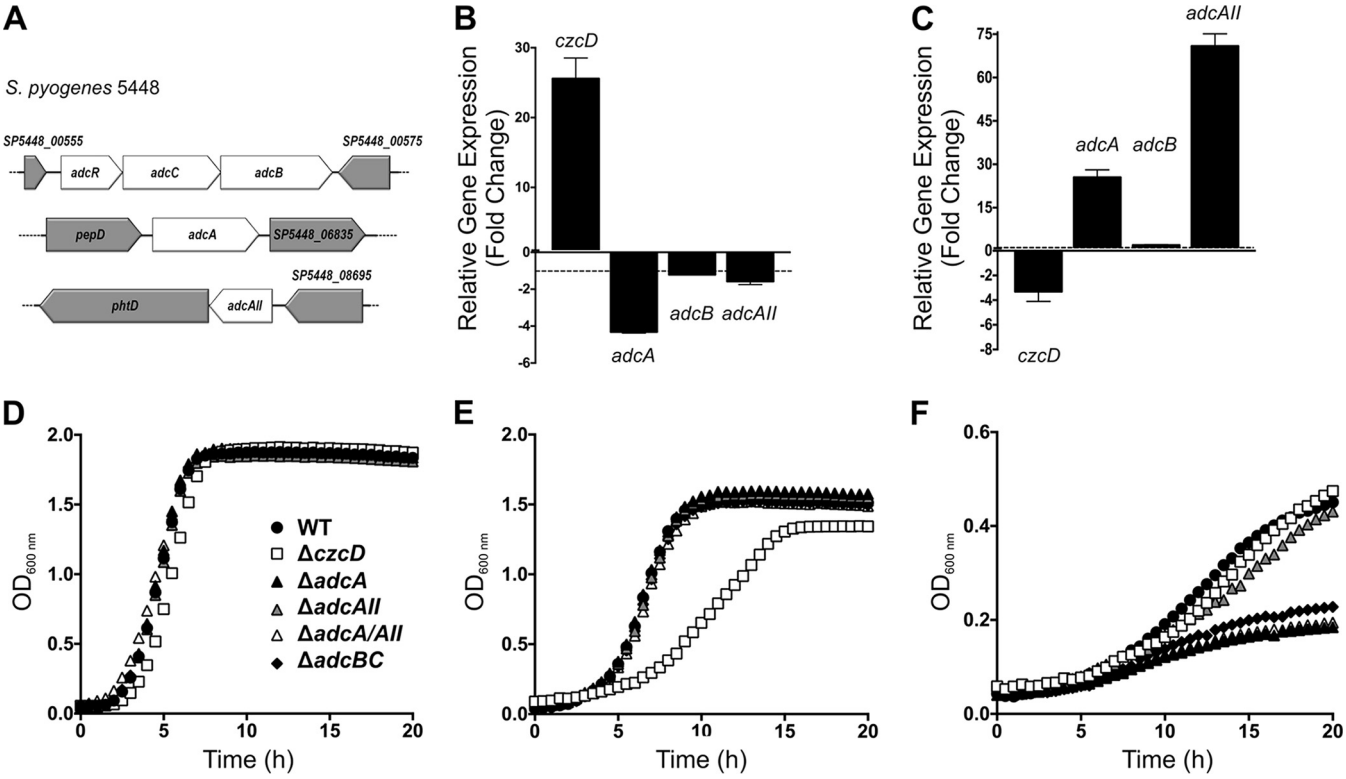

FIG 1 Zinc acquisition and efflux in GAS. (A) Diagram representation of the gene locations of *adcR*, *adcC*, *adcB*, *adcA*, and *adcAII* in the GAS 5448 genome. Gene sizes are to scale. (B, C) Comparison of the relative levels of expression of zinc export (*czcD*) and zinc import (*adcA*, *adcB*, and *adcAII*) genes in strain 5448 wild type under zinc excess (1 mM $ZnSO_4$) (B) or zinc-limiting (65 μM TPEN) (C) conditions. Error bars show standard deviations of the results from 3 independent experiments. The relative levels of gene expression were calculated using the cycle threshold ($2^{-\Delta\Delta CT}$) method, with *gyrA* as the reference gene, and are expressed as fold changes in expression in GAS grown under zinc overload or -limiting conditions compared to the expression in GAS grown in THY alone. Two-way ANOVA was used to compare the relative levels of gene expression under zinc excess or zinc-limiting conditions to their expression in THY ($P < 0.0001$). (D to F) Comparison of the growth of 5448 WT and isogenic deletion mutants (Δ*czcD*, Δ*adcA*, Δ*adcAII*, Δ*adcA* Δ*adcAII*, and Δ*adcBC*) in Todd Hewitt broth plus 1% yeast extract (THY) (D) and THY supplemented with 1 mM zinc sulfate (E) or 65 μM TPEN (F). Graph is representative of 3 independent experiments.

than in mice infected with either the Δ*czcD* or Δ*adcA* Δ*adcAII* mutant (Fig. 2A, 24 h) ($P < 0.05$), but as the time course of infection progressed, only mice infected with the Δ*adcA* Δ*adcAII* mutant developed significantly smaller skin lesions than did mice infected with 5448 WT (Fig. 2A, 48 h and 96 h) ($P < 0.05$). However, there were no significant differences in the lesion sizes of mice infected with the Δ*czcD* mutant and mice infected with the Δ*adcA* Δ*adcAII* mutant at either of the time points (Fig. 2A) ($P > 0.05$).

We also determined the capacity of GAS to disseminate into the bloodstream postinfection. As early as 24 h postinfection, GAS WT had disseminated into the bloodstream of mice, while there was no detectable recovery of the Δ*czcD* or Δ*adcA* Δ*adcAII* mutant at 24 h or 48 h postinfection (Fig. 2B). The Δ*czcD* mutant was recovered from blood at 96 h postinfection (Fig. 2B), but in contrast, the Δ*adcA* Δ*adcAII* mutant was only rarely recovered, indicating that loss of *adcA* and *adcAII* considerably reduced the dissemination of GAS into the blood (Fig. 2B, 96 h) ($P < 0.05$). Furthermore, at 96 h postinfection, the recovery of the Δ*adcA* Δ*adcAII* mutant was significantly less than the recovery of the Δ*czcD* mutant (Fig. 2B) ($P < 0.05$), indicating that the Δ*adcA* Δ*adcAII* mutant has an even more reduced ability to disseminate into the blood.

The virulence of 5448 WT compared to that of the Δ*czcD* and Δ*adcA* Δ*adcAII* mutants was additionally assessed by monitoring the survival of human-plasminogenized mice after subcutaneous infection. The Δ*czcD* mutant and the Δ*adcA* Δ*adcAII* mutant were less virulent than 5448 GAS WT, with the Δ*adcA* Δ*adcAII* mutant showing the greatest attenuation of virulence (Fig. 2C). In addition, the Δ*adcA* Δ*adcAII* mutant was signifi-

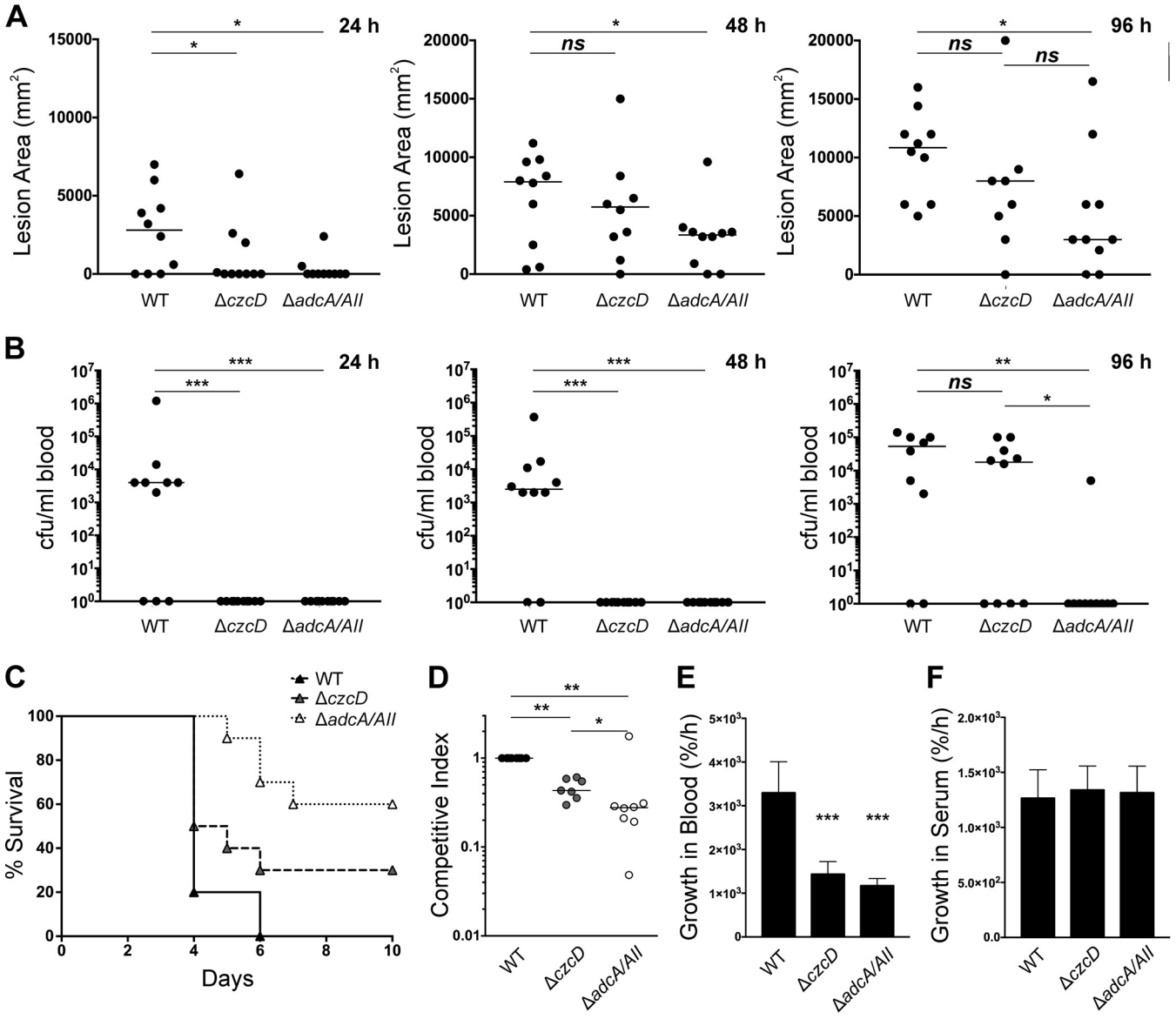

FIG 2 GAS zinc homeostasis is important for skin colonization, blood dissemination, and virulence. (A) Areas of lesions (dimensions of the cross section) formed on human-plasminogenized mice 24, 48, and 96 h after subcutaneous infection with 5448 WT and zinc export (Δ*czcD*) and zinc import (Δ*adcA* Δ*adcAII*) deletion mutants at a dose of 2×10^7 CFU ($n = 10$). One-way ANOVA of the results was performed for 5448 WT versus each mutant and for the zinc export (Δ*czcD*) versus the zinc import (Δ*adcA* Δ*adcAII*) mutant. *, $P < 0.05$; *ns*, not significant. Horizontal bars represent the median lesion sizes. (B) Total colonies per milliliter of blood from human-plasminogenized mice 24, 48, and 96 h after subcutaneous infection with 5448 WT and zinc export (Δ*czcD*) and zinc import (Δ*adcA* Δ*adcAII*) deletion mutants at a dose of 2×10^7 CFU ($n = 10$). One-way ANOVA of the results was performed for 5448 WT versus each mutant and for the zinc export (Δ*czcD*) versus the zinc import (Δ*adcA* Δ*adcAII*) mutant. *, $P < 0.05$; **, $P < 0.01$; ***, $P < 0.001$; *ns*, not significant. Horizontal bars represent the median numbers of CFU/ml blood. (C) Virulence survival curve showing survival of human-plasminogenized mice after subcutaneous infection with 5448 WT and zinc export (Δ*czcD*) and zinc import (Δ*adcA* Δ*adcAII*) deletion mutants at a dose of 2×10^7 CFU ($n = 10$). (D) Competitive skin colonization assay was performed using 50:50 mixture of WT and Δ*czcD* mutant or WT and Δ*adcA* Δ*adcAII* mutant subcutaneously injected into human plasminogenized mice. Colonies were enumerated 3 days postinfection on selective THY agar plates (dose $= 2 \times 10^7$ CFU, $n = 8$). Competitive indices were calculated as total number of mutant colonies divided by total number of 5448 WT colonies. One-way ANOVA was performed on the competitive indices for both mutants compared to the WT and for the zinc export (Δ*czcD*) versus the zinc import (Δ*adcA* Δ*adcAII*) mutant. *, $P < 0.05$; **, $P < 0.005$. (E) Growth of 5448 WT and zinc export (Δ*czcD*) and zinc import (Δ*adcA* Δ*adcAII*) deletion mutants in human blood. Bacterial cells were enumerated at $T = 0$ and $T = 3$ h, and multiplicities of growth calculated as cell counts at $T = 3$ h divided by cell counts at $T = 0$ h. One-way ANOVA of the results was performed for 5448 WT versus each mutant. ***, $P < 0.001$. (F) Growth of 5448 WT and zinc export (Δ*czcD*) and zinc import (Δ*adcA* Δ*adcAII*) deletion mutants in human serum. Bacterial cells were enumerated at $T = 0$ and $T = 3$ h, and multiplicities of growth calculated as cell counts at $T = 3$ h divided by cell counts at $T = 0$ h. One-way ANOVA of the results was performed for 5448 WT versus each mutant.

cantly less virulent than the Δ*czcD* mutant (Fig. 2C) ($P < 0.05$). In order to assess the ability to colonize skin, human-plasminogenized mice were also infected subcutaneously with a mixture of 50:50 WT/mutant, the lesion excised, and GAS colonies enumerated 3 days postinfection. The competitive index indicated that both the Δ*czcD*

and Δ*adcA* Δ*adcAII* mutants were less competitive than 5448 WT in colonizing the skin lesion, with the Δ*adcA* Δ*adcAII* mutant being the least competitive (Fig. 2D, WT versus Δ*czcD* mutant [$P < 0.05$], WT versus Δ*adcA* Δ*adcAII* mutant [$P < 0.05$], and Δ*czcD* mutant versus Δ*adcA* Δ*adcAII* mutant [$P < 0.05$]). The Δ*czcD* and Δ*adcA* Δ*adcAII* mutants both exhibited reduced growth compared to that of 5448 WT in nonimmune human blood (Fig. 2E), whereas in human serum, there was no difference in growth between any of the three strains (Fig. 2F). Taken together, these results indicate that, even though zinc import and export are both important for GAS infection, the deletion mutations in the zinc import system appear to cause a more severe virulence defect and innate immune cells may play an important role in this process.

High levels of zinc and calprotectin are found at the site of GAS infection. Tissue histology was performed on skin samples from healthy and infected human-plasminogenized mice 3 days after subcutaneous infection. As an additional control, we also examined samples of skin adjacent to the lesion in infected mice. The skin samples of uninfected mice and the control adjacent-skin samples of infected mice were intact and healthy (Fig. 3A, B, F, and G). However, infected-skin lesions had damage to the epidermis, dermis, and hypodermis layers (Fig. 3C). Furthermore, there was an influx of innate immune cells into the infected lesions (Fig. 3D and E). Immunofluorescence histology staining identified the presence of GAS, neutrophils, and calprotectin at the site of infection (Fig. 3H). We also determined the total zinc concentration at the site of the infection, using inductively coupled plasma mass spectrometry (ICP-MS) analysis of the control skin samples and the infected-skin-lesion and adjacent-skin samples of infected mice 3 days after subcutaneous infection. The entire lesions were excised, as well as healthy adjacent skin from infected mice and control skin samples from uninfected mice, and the total zinc values were normalized to the weight of the lesion or skin samples. ICP-MS showed that total zinc content is increased significantly at the site of GAS infection (Fig. 3I) ($P < 0.05$). Since innate immune cells, such as neutrophils, are known to be rich in zinc (27), this increase in zinc coincides with the influx of innate immune cells, such as neutrophils, to the site of infection (Fig. 3E and H). However, even though there is an increased level of total zinc at the site of infection due to white blood cell influx, zinc is potentially unavailable to the bacterial cells from the extracellular *milieu* due to sequestration by calprotectin, which creates a zinc-limiting environment.

Intracellular zinc intoxication by neutrophils and extracellular chelation of zinc to control GAS infection. To gain insight into the zinc-homeostatic response of GAS at the site of infection, we first examined the transcription of different metal transporter genes in the 5448 WT strain following a 30-min exposure to human neutrophils. Confirming previous studies, the relative level of gene expression of *czcD* was increased over 2-fold after neutrophil exposure (Fig. 4A) (11). On the other hand, the genes encoding zinc import, *adcA*, *adcB*, and *adcAII*, were 1.5- to 2-fold decreased after neutrophil exposure (Fig. 4A). No changes were observed in genes encoding copper export (*copA*), manganese import (*mtsA*), manganese export (*mntE*), and iron export (*pmtA*). These results indicate that GAS is encountering zinc overload conditions within the neutrophils. The survival of the Δ*czcD* and Δ*adcA* Δ*adcAII* mutants was compared to that of 5448 WT in the presence of human neutrophils. Only the zinc export mutant was significantly more susceptible to human neutrophil killing than 5448 WT (Fig. 4B) ($P < 0.05$). Similarly, in a competition assay where the WT and mutant were combined at a 50:50 ratio and exposed to human neutrophils, only the *czcD* mutant was significantly less competitive than the 5448 WT (Fig. 4C) ($P < 0.05$).

To examine extracellular mechanisms used to control infection, the human neutrophil assay was performed with pretreatment using cytochalasin D, which inhibits actin polymerization, thereby preventing phagocytosis and, thus, blocking intracellular killing of GAS. The results showed that the Δ*czcD* mutant was able to survive extracellular human neutrophil control mechanisms similarly to 5448 WT (Fig. 4D). In contrast, the Δ*adcA* Δ*adcAII* mutant had significantly reduced survival (Fig. 4D) ($P < 0.05$). Furthermore, the 5448 Δ*sda1* mutant, which is deficient in the DNase responsible for the

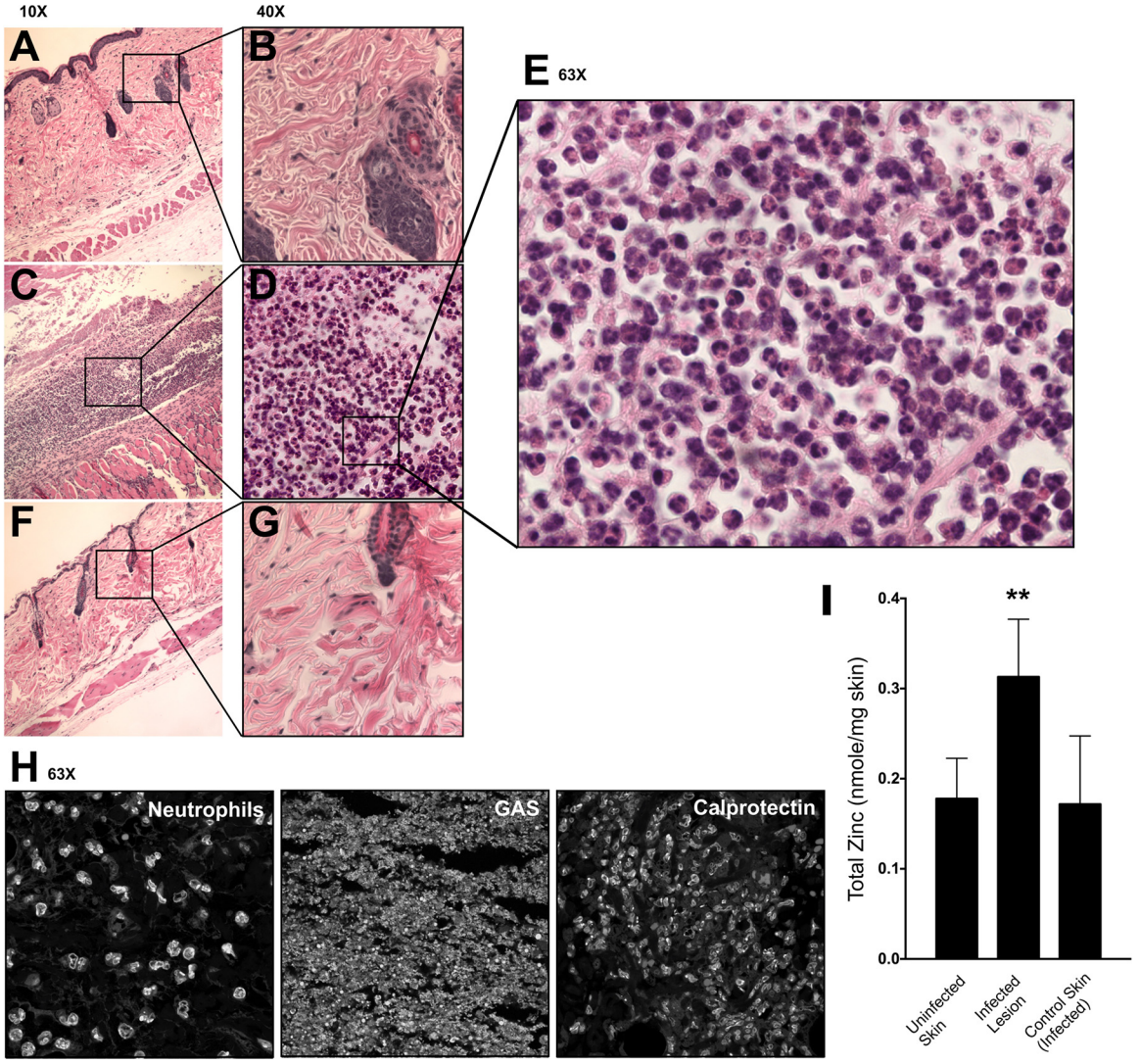

FIG 3 Influx of neutrophils and zinc at the site of skin colonization. (A, B) Tissue histology of healthy human-plasminogenized-mouse skin, shown at ×10 (A) and ×40 (B) magnification. (C to E) Tissue histology of human-plasminogenized-mouse infected-skin lesion 3 days after subcutaneous infection with 5448 WT, shown at ×10 (C), ×40 (D), and ×63 (E) magnification. (F, G) Tissue histology of human-plasminogenized-mouse control skin adjacent to the lesion 3 days after subcutaneous infection with 5448 WT, shown at ×10 (F) and ×40 (G) magnification. Mice were infected with a dose of 2×10^7 CFU. Images are representative of the results from 3 independent mice. (H) Immunofluorescence histology identifying the presence of neutrophils (anti-CD63 antibody), GAS (anti-group A carbohydrate antibody), and calprotectin (anti-S100A9 antibody) in human-plasminogenized-mouse infected-skin lesion 3 days after subcutaneous infection with 5448 WT, shown at ×63 magnification (dose = 2×10^7 CFU). (I) Total zinc contents from skin of uninfected mice, infected-skin lesions of human-plasminogenized mice 3 days after subcutaneous infection with 5448 WT, and control skin adjacent to the lesions of infected mice (dose = 2×10^7 CFU). Total zinc content was normalized to the weight of the sample. One-way ANOVA of the results was performed for total zinc from skin of uninfected versus infected mice. **, $P < 0.005$.

degradation of neutrophil extracellular traps (NETs) during extracellular neutrophil killing (28), also demonstrated reduced survival (Fig. 4D). In the absence of cytochalasin D, only the Δ*czcD* and Δ*sda1* mutants had reduced survival compared to that of 5448 WT under normal human neutrophil killing conditions (Fig. 4D). Together, these results indicate that zinc toxicity is an intracellular neutrophil killing event, while zinc limitation is an extracellular event.

Zinc is stored within neutrophil lysosomes and azurophilic granules. Currently, there are a total of 24 known mammalian metal transporters (10 from the ZnT [SLC30A] and 14 from the ZIP [SLC39A] family) identified as being involved in the transport of zinc and other metals within mammalian cells (7). Reverse transcriptase PCR was performed using human neutrophils to identify and confirm the presence of zinc or metal transporters, storage proteins, and regulators (Table 1).

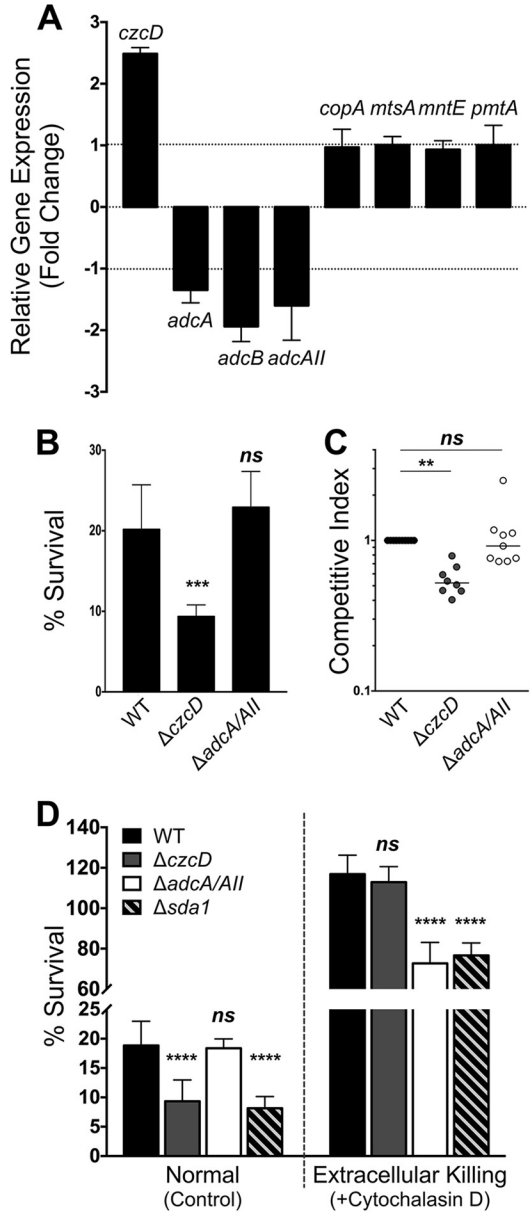

FIG 4 Intracellular zinc toxicity within human neutrophils. (A) Relative expression levels of GAS metal transporter genes in 5448 WT after contact with human neutrophils. Genes tested included genes coding for zinc export (*czcD*), zinc import (*adcA*, *adcB*, and *adcAII*), copper export (*copA*), manganese import (*mtsA*), manganese export (*mntE*), and iron export (*pmtA*). Error bars show standard deviations of the results of 3 independent experiments; relative expression is expressed as fold change of gene expression in GAS in contact with neutrophils divided by gene expression in control GAS. Relative gene expression was calculated using the $2^{-\Delta\Delta CT}$ method, with *gyrA* as the reference gene. (B) Human neutrophil killing assay showing the percent survival of 5448 WT and zinc export (Δ*czcD*) and zinc import (Δ*adcA* Δ*adcAII*) mutants following coculture with human neutrophils *in vitro*. Error bars show standard deviations of the results of 3 independent experiments. One-way ANOVA of the results was performed for the WT versus the mutants. ***, $P < 0.001$; *ns*, not significant. (C) Competitive human neutrophil killing assay was performed using 50:50 mixtures of WT and Δ*czcD* mutant or WT and Δ*adcA* Δ*adcAII* mutant. Colonies were enumerated on selective THY agar plates after 30 min of incubation with human neutrophils. Competitive indices were calculated as total numbers of mutant colonies divided by total numbers of 5448 WT colonies. One-way ANOVA was performed on the competitive indices for both mutants compared to the WT. **, $P < 0.005$; *ns*, not significant. (D) Human neutrophil killing assay in the absence and presence of 10 μg/ml cytochalasin D. Cytochalasin D inhibits actin polymerization, hence preventing phagocytosis and intracellular uptake of bacteria. Results show the percent survival of 5448 WT and zinc export (Δ*czcD*), zinc import (Δ*adcA* Δ*adcAII*), and DNase1 (Δ*sda1*) deletion mutants following coculture with human neutrophils *in vitro*. Error bars show standard deviations of the results of 3 independent experiments. One-way ANOVA of the results was performed for the WT versus the mutants. ****, $P < 0.0001$; *ns*, not significant.

TABLE 1 List of zinc transport and related genes expressed in human neutrophils

Function, protein family	Protein encoded	Presence of gene[a]
Metal transport		
ZnT (SLC30A)	ZnT1	+
	ZnT2	+
	ZnT3	
	ZnT4	+
	ZnT5	
	ZnT6	
	ZnT7	+
	ZnT8	+
	ZnT9	+
	ZnT10	
ZIP (SLC39A)	ZIP1	+
	ZIP2	
	ZIP3	+
	ZIP4	+
	ZIP5	
	ZIP6	+
	ZIP7	+
	ZIP8	+
	ZIP9	+
	ZIP10	+
	ZIP11	+
	ZIP12	
	ZIP13	+
	ZIP14	+
Zinc storage		
Metallothionein	MT1A	
	MT1B	+
	MT1E	+
	MT1F	+
	MT1G	
	MT1H	
	MT1X	+
	MT2	+
	MT3	
	MT4	+
Other functions		
Metal regulation	MTF-1	+
	MTF-2	+
Copper transport	ATP7A	+
γ-Glutamylcysteine synthetase	GCS	+
Housekeeping	RPL32	+
	HRPT1	+

[a]+, gene is present in human neutrophils.

Next, relative gene expression was assessed to test for changes in the expression of these ZnT and ZIP zinc transporters during infection with GAS 5448 WT cells in human neutrophils, to determine whether induction of genes involved in host zinc mobilization was occurring during an infection. The results demonstrate that there are no significant changes in expression for any of the genes encoding the zinc transporters after half an hour of infection with GAS (Fig. 5A). This indicates that the response to bacterial infection by human neutrophils is not transcriptionally regulated.

Next, confocal immunofluorescence microscopy was performed to identify the vesicular location of zinc within the human neutrophils. Confocal microscopy identified that the zinc signal {2-methyl-8-[(4-methylphenyl)sulfonylamino]-6-(ethyloxycarbonylmethyloxy)quinoline (Zinquin)} colocalized with both the lysosome (anti-Lamp 1 antibody) and azurophilic (anti-proteinase-3 antibody) granules (see Fig. S1 in the supplemental material). In order to confirm colocalization of zinc with the lysosome and azurophilic granules, superresolution microscopy was performed using Delta-Vision OMX 3D-SIM technology. Superresolution microscopy

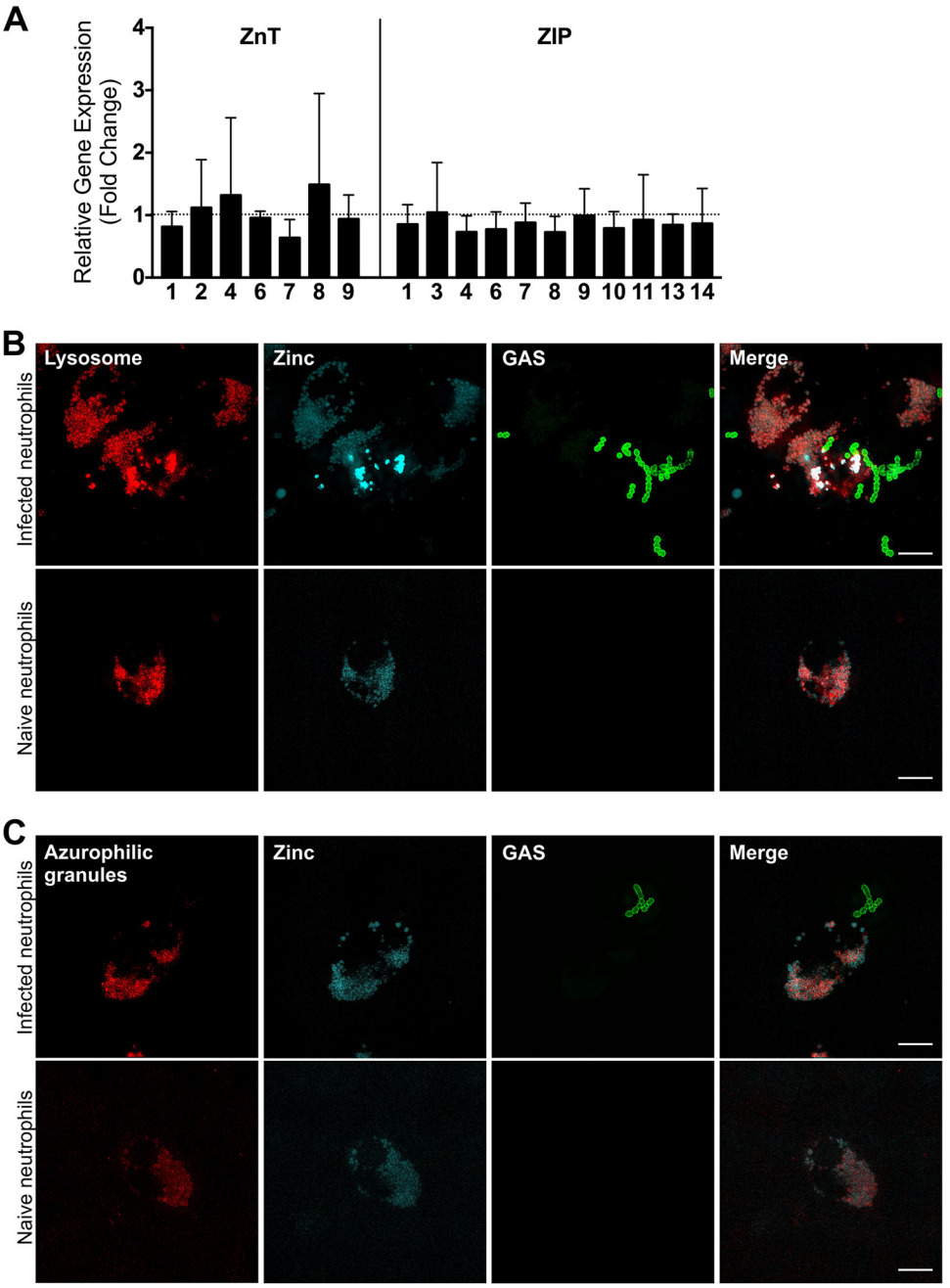

FIG 5 Zinc is localized to the lysosome and azurophilic granules of human neutrophils. (A) Relative expression levels of genes encoding mammalian zinc metal transporters in human neutrophils after contact with GAS. Genes tested included *znt1*, *-2*, *-4*, *-6*, *-7*, *-8*, and *-9* and *zip1*, *-3*, *-4*, *-6*, *-7*, *-8*, *-9*, *-10*, *-12*, and *-14*. Error bars show standard deviations of the results of 8 independent experiments using neutrophils from at least 3 different blood donors; relative expression is expressed as fold change of gene expression in neutrophils in contact with 5448 WT GAS divided by gene expression in naive neutrophils. Relative gene expression was calculated using the $2^{-\Delta\Delta CT}$ method, with *RPL32* and *HRPT1* as the reference genes. (B) Superresolution immunofluorescence micrograph demonstrating the colocalization of zinc (Zinquin; cyan) and lysosome (anti-LAMP1 antibody; red) in human neutrophils infected with 5448 WT GAS (anti-group A carbohydrate antibody; green) and in naive neutrophils. (C) Superresolution immunofluorescence micrograph demonstrating the colocalization of zinc (Zinquin; cyan) and azurophilic granules (anti-proteinase 3 antibody; red) in human neutrophils infected with 5448 WT GAS (anti-group A carbohydrate antibody; green) and in naive neutrophils.

confirmed that zinc (Zinquin) colocalized with lysosomal markers in both infected and naive neutrophils (Fig. 5B; Videos S1 and S2). Similarly, zinc was also found to colocalize with the azurophilic granules in both infected and naive neutrophils (Fig. 5C; Videos S3 and S4). Three-dimensional videos of the high-resolution mi-

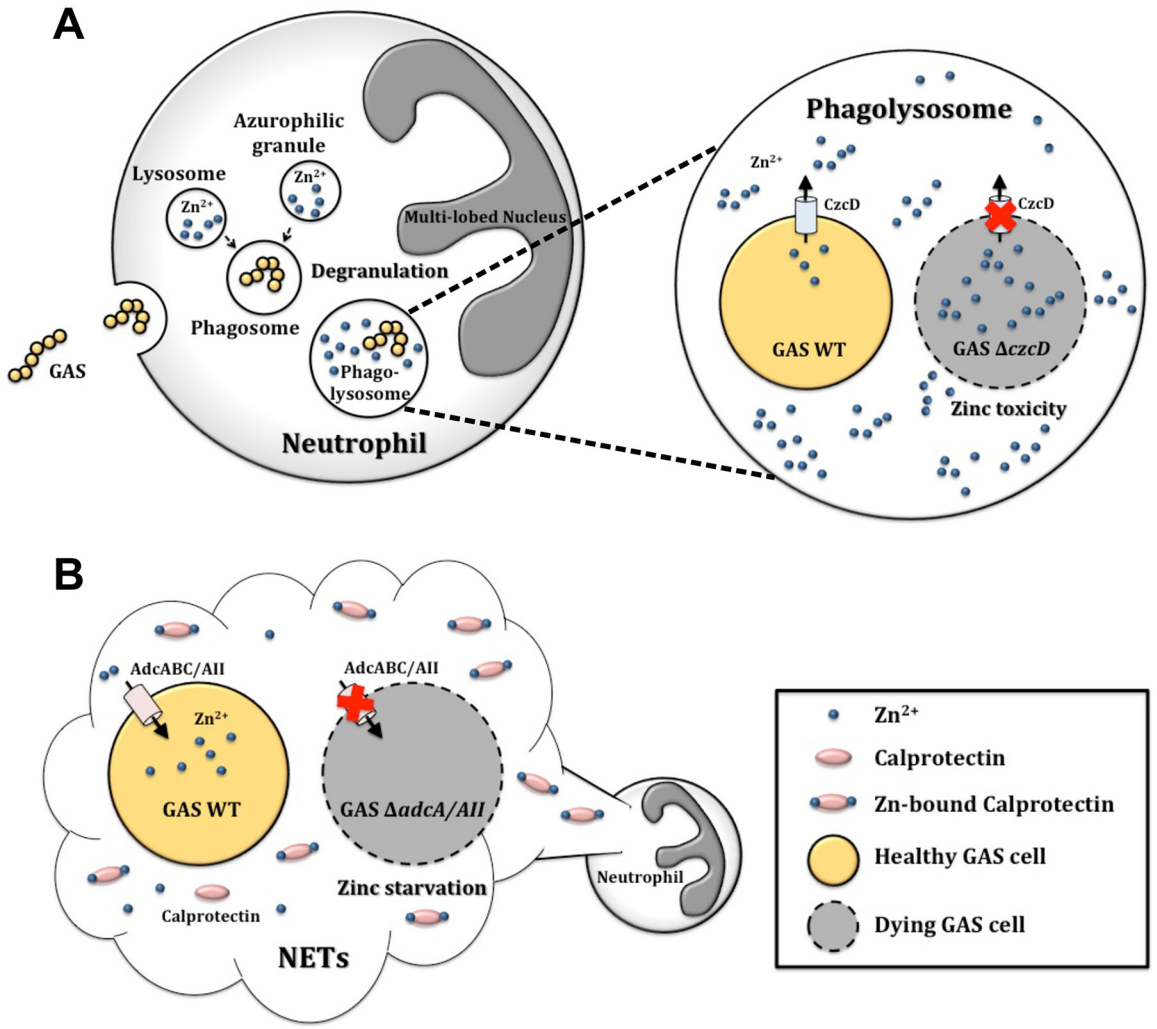

FIG 6 Proposed model of zinc utilization during neutrophil killing of GAS cells. (A) Intracellular zinc toxicity within human neutrophils. GAS cells are phagocytosed into the phagosome, which fuses with the zinc-rich lysosomes to form the phagolysosome. The azurophilic granules also degranulate, releasing their contents, which include zinc, into the phagolysosome. As a consequence, a high-zinc environment is formed within the phagolysosome that results in zinc toxicity to the GAS cells. Within the phagolysosome, a zinc export-deficient mutant (Δ*czcD*) is unable to export the excess zinc, and hence, it will experience zinc toxicity and cell death. (B) Extracellular zinc starvation (nutritional immunity) as a result of calprotectin. The abundance of zinc-chelating calprotectin released in neutrophil extracellular traps (NETs) results in an extracellular zinc-limiting environment. GAS cells can be trapped within NETs, and a zinc import deletion mutant (Δ*adcA* Δ*adcAII*) that is unable to acquire zinc for growth will therefore experience zinc starvation and cell death.

croscopy are presented in the supplemental material. These results lead us to hypothesize that zinc is possibly prepackaged into lysosomes and azurophilic granules prior to infection (Fig. 6A). Therefore, during infection, when the azurophilic granules degranulate and lysosomes fuse with the phagosome to form the phagolysosome, GAS will encounter high levels of intracellular zinc (Fig. 6A).

DISCUSSION

Zinc is known to be important for the control of various bacterial infections. Zinc deficiency in humans and zinc-deficient murine model systems have been shown to result in increased susceptibility to infection (29–32). Studies have shown that zinc deficiency results in impaired phagocytosis and intracellular killing of pathogens but that this is readily reversible by zinc supplementation (33–36). However, it is also established that at local sites of infection, such as in tissue abscesses, zinc and manganese limitation as a consequence of the action of calprotectin restricts bacterial growth, giving rise to the concept of nutritional immunity in relation to these two metals (3, 5). The apparent paradox that both

zinc sufficiency and zinc limitation are required for the management of bacterial infection by the host is resolvable if we consider that, during infection, there are changes in zinc concentrations within the host, both spatially and temporally. In this study, we have used a set of isogenic mutant strains in the same genetic background (M1T1 GAS strain 5448) to examine the effects of loss of zinc uptake and zinc efflux on pathogenesis.

Zinc has been directly implicated in the intoxication of bacterial pathogens within innate immune cells (11–13), and elevated zinc levels have been recorded in serum and tissues of infected mice (10). Here, elevated zinc levels were recorded in the GAS-infected mouse skin (Fig. 3I). It is therefore not surprising that a GAS Δ*czcD* (zinc export) mutant has reduced virulence in both *in vitro* and *in vivo* assays, confirming our previous study (11). However, zinc is an important essential nutrient in bacteria, and it is the most abundant transition metal ion, with approximately 6% of proteins being zinc bound (29, 37). As a consequence, most bacteria have at least one zinc acquisition system to ensure proper function of proteins and enzymes. GAS possesses the Adc system to overcome zinc limitation (9, 18). This system is comprised of the surfaced-exposed zinc-binding protein AdcA, the permease AdcB, and the cytosolic ATPase AdcC, as well as a second zinc-binding protein, AdcAII, all of which are regulated by AdcR (18). Studies have shown that deletions of various components of the Adc proteins have resulted in reduced virulence in GAS and other streptococcal species (9, 18, 19, 22–24). It is therefore apparent that during an infection process, the pathogen will encounter zinc limitation and require a zinc uptake system. Here, we examine the various stages of infection that utilize either zinc toxicity or zinc limitation as a pathogen control strategy.

The Adc systems in GAS and *Streptococcus pneumoniae* are well characterized, and studies have shown that both AdcA and AdcAII are zinc specific and have potentially redundant functions (9, 20, 22, 23). Previous studies have shown that GAS *adcAII* is more strongly upregulated than *adcA* under zinc-limiting conditions in the GAS *emm3* strain MGAS10870 (18), similar to our results using the *emm1* 5448 genetic background (Fig. 1C). In *S. pneumoniae*, studies have also noted that deletion of both *adcA* and *adcAII* was required to completely abolish zinc import (22, 23); however, in the GAS *emm1* strain MGAS5005, deletion of either *adcA* or *adcAII* was sufficient to inhibit growth in zinc-limiting medium (20). In contrast, our data demonstrated that AdcA appears to be the main zinc import system under the zinc-limiting growth condition tested (Fig. 1F), even though gene expression data indicate that the *adcAII* gene is the most upregulated (Fig. 1C). The differences in these studies could be due to differences in the growth media, in the streptococcal species characterized, and in the GAS strains examined (MGAS5005 compared to 5448). Therefore, to ensure that we were working with a zinc import-deficient mutant, we proceeded to use the 5448 Δ*adcA* Δ*adcAII* double deletion mutant for the subsequent virulence assays (Fig. 1F).

The second GAS zinc-binding protein, AdcAII (19–21, 38) has been previously shown to be upregulated over 500-fold in the GAS *emm14* strain HSC5 during a murine soft tissue infection (39), and the *adcAII* deletion mutant was highly attenuated in the ability to form a skin lesion in the GAS *emm14* strain HSC5 (19). This is consistent with our data showing that the Δ*adcA* Δ*adcAII* double mutant formed significantly smaller lesions than the Δ*czcD* mutant and 5448 WT (Fig. 2A). Additionally, the Δ*adcA* Δ*adcAII* mutant was more attenuated than the Δ*czcD* mutant in the ability to colonize the skin, disseminate into the blood, and cause lethal infection in mice (Fig. 2). This indicates that zinc acquisition is essential for GAS skin colonization and virulence. Previously, an *adcC* deletion mutant in the GAS *emm3* strain MGAS10870 background was shown to be attenuated in both soft tissue infection and invasive infection (9). Furthermore, in *Streptococcus agalactiae*, an *adcAII* deletion mutant demonstrated reduced invasion (40). In *S. pneumoniae*, an *adcA* Δ*adcAII* mutant was less virulent in both colonization and invasion mouse models and also showed reduced ability to grow in bronchoalveolar lavage fluid and in human serum (22, 23). Through the use of transposon mutagenesis screens and Tn-Seq, it has been found in GAS strain 5448 that *adcC* is

important for growth in blood and that *adcA* is required for fitness in murine skin and soft tissue infection models (25, 26).

Neutrophils migrate from circulating blood to infected tissues, and upon arrival, can eliminate the invading pathogen by a number of methods, one of which is via neutrophil extracellular traps (NETs) (41). The release of NETs entraps the pathogen and creates an environment with a high concentration of antimicrobials, such as calprotectin (42). Calprotectin makes up approximately 40 to 60% of the neutrophil cytosolic protein content (43, 44) and restricts the growth of various bacterial pathogens, such as *Staphylococcus aureus*, by chelating zinc and manganese (5). In this study, calprotectin was abundant at the site of GAS skin colonization (Fig. 3H). The concentration of calprotectin at sites of infection can be as high as 500 μg/ml (45). Purified calprotectin has been shown to inhibit the growth of GAS *emm3* strain MGAS10870 *in vitro* (9). High calprotectin levels have also been measured after both intramuscular and subcutaneous infection with GAS (9). Here, we observed that the Δ*adcA* Δ*adcAII* zinc import mutant was also highly attenuated in the mouse model of infection (Fig. 2).

Neutrophils can also utilize phagocytosis and intracellular killing for pathogen removal. We have previously shown that GAS encounters high levels of zinc within human neutrophils (11). This is consistent with the upregulation of *czcD* and downregulation of *adcAI*, *adcB*, and *adcAII* in GAS cells when in contact with human neutrophils (Fig. 4A). Furthermore, the Δ*adcA* Δ*adcAII* mutant only demonstrated reduced survival compared to that of 5448 WT during extracellular killing by neutrophils in the presence of cytochalasin D (Fig. 4B to D). This result is potentially reflective of the action of calprotectin. Calprotectin responds to extracellular calcium ions to become a potent chelator of zinc and manganese in the extracellular space (8). In contrast, intracellular calprotectin is maintained in the nonchelating form due to low calcium levels in the cytoplasm and is only active when released from neutrophils. Furthermore, the GAS cells are spatially separated from calprotectin, since they are contained within the phagolysosome and intracellular calprotectin is stored in the cytoplasm (43).

Zinc mobilization occurs within mammalian cells via a complicated combination of 24 metal transporters, of which 10 belong to the ZnT (SLC30) family and 14 belong to the ZIP (SLC39) family (7, 46, 47). The ZnT proteins transport zinc out of the cytoplasm, while the ZIP proteins transport zinc into the cytoplasm (7). Gene expression studies indicated that none of these zinc transporter families were differentially regulated in human neutrophils during GAS infection (Fig. 5A). However, this does not exclude the possibility of protein expression changes during an infection. Neutrophils are rapidly turned over in the host, have been shown to be a rich source of zinc, and are considered a reliable indicator of zinc status in humans (27, 48). Thus, we hypothesize that the zinc is prepackaged within compartments of the neutrophil prior to infection. Therefore, an increase in the total zinc levels in the infected-skin lesions of mice corresponds to the increased numbers of neutrophils at the site of infection (Fig. 3E and I). However, as mentioned earlier, the abundance of calprotectin restricted the availability of zinc.

Within the neutrophil, we have shown that zinc is localized to lysosomes and azurophilic granules (Fig. 5B and C). To date, zinc has been shown to accumulate in lysosomes of mammary gland cells via the action of ZnT2 (49), in lysosomes of T cells via ZIP8 (47), and in the late endosomes and lysosomes of human macrophages (12). Here, we report zinc accumulation within lysosomes and azurophilic granules of human neutrophils. We therefore suggest that during phagocytosis, lysosomes fuse with the phagosome and azurophilic granules degranulate into the phagolysosome, resulting in increased zinc toxicity to the pathogen (Fig. 6A). In such instances, the zinc export-deficient mutant (Δ*czcD*) would be unable to cope with the increased zinc levels in the phagolysosome and bacterial cell death would occur (Fig. 6A). On the other hand, when neutrophils release NETs during extracellular killing, the GAS cells are entrapped, while calprotectin may contribute to restricting zinc availability, and therefore, the zinc import-deficient mutant (Δ*adcA* Δ*adcAII*) would experience zinc starvation (Fig. 6B).

Combined, our results indicate that the role zinc plays in the control of bacterial

infection is complex. Zinc limitation is likely the norm in extracellular situations where calprotectin may serve to restrict zinc availability; in contrast, zinc intoxication of bacterial pathogens is likely an intracellular process that occurs in neutrophils and macrophages. The way in which the movement of zinc during infection is coordinated to deliver direct antimicrobial activity, as well as control of the inflammatory response, will be of interest for future studies. In terms of the relative importance of zinc acquisition and zinc tolerance in bacterial pathogenesis, our data suggest that optimized zinc homeostasis defines the fitness of a bacterial pathogen.

MATERIALS AND METHODS

Bacterial strains and growth conditions. *S. pyogenes* M1T1 strain 5448 (50) and isogenic derivatives were cultured routinely in Todd-Hewitt (Oxoid) medium supplemented with 1% yeast extract (Merck) (THY). Where required, spectinomycin was used at a concentration of 100 μg/ml, kanamycin at 200 μg/ml, and erythromycin at 2 μg/ml. Both liquid and agar cultures were grown at 37°C. *E. coli* MC1061 (51) was grown in Luria-Bertani (LB) broth and supplemented with spectinomycin (100 μg/ml) and erythromycin (500 μg/ml) when required. Bacterial strains used in this study are listed in Table S1 in the supplemental material.

DNA manipulation and genetic techniques. GAS mutants were constructed as previously described unless otherwise indicated (11). Electrotransformation was carried out using standard protocols described previously (11). All constructs and knockout strains were confirmed by DNA sequencing done at the Australian Equine Genetics Research Centre, The University of Queensland. In addition, M protein levels and capsule levels were similar to the levels in the wild type (data not shown). Plasmids and primers used in this study are listed in Tables S1 and S2, respectively.

Growth curve analysis. Growth assays were performed as previously described (11). The growing cultures were diluted to an optical density at 600 nm (OD_{600}) of 0.01 in fresh THY (in the presence of either 1 mM $ZnSO_4 \cdot 7H_2O$ or 65 μM TPEN; Sigma) in a 96-well microtiter plate. The cells were grown statically, and the OD_{600} measured every 30 min in a CLARIOstar microplate reader (BMG Labtech).

Quantitative gene expression studies. GAS RNA was isolated from cells harvested during the desired growth phase (grown in the presence or absence of 1 mM zinc, 50 μM TPEN, or human neutrophils). RNA was isolated, and quantitative PCR was performed based on a previously described protocol, using *gyrA* as the reference gene (11). Human neutrophil RNA was isolated from uninfected neutrophils and neutrophils infected with GAS according to the RNeasy plus minikit (Qiagen) instructions and converted to cDNA (SuperScript III first-strand synthesis system; Thermo Fisher). Quantitative PCR was performed as described above, using *RPL32* and *HRPT1* as reference genes (52). Primers used for the amplification of ZIP and ZnT genes are described elsewhere (53).

Virulence of GAS in a humanized-plasminogen transgenic mouse model. Transgenic humanized-plasminogen (*AlbPLG1*$^{+/-}$) mice (54) were subcutaneously infected ($n = 10$) with a dose of 2×10^7 CFU, and virulence was assessed as previously described (11). Blood dissemination was determined by counting bacterial loads from blood samples collected every 24 h postinfection for up to 5 days. Lesion areas were determined by measuring the cross section of the lesion every 24 h postinfection for up to 5 days. In the competition skin infection assays, mice ($n = 8$) were subcutaneously infected with 50:50 WT/mutant mixtures at a dose of 2×10^7 CFU. Bacterial load was determined 72 h postinfection by enumerating colonies plated onto selective THY agar plates. The competitive index was a measure of total mutant colonies over total 5448 WT colonies recovered from the skin.

Growth of GAS in human blood and serum. Growth in human blood was performed in biological triplicates using mid-logarithmic-phase ($A_{600} = 0.4$) GAS diluted 1:10 in whole human blood that was collected in sodium citrate blood collection vials, with incubation at 37°C on a rotary wheel for 3 h. Bacterial cells were enumerated at time zero ($T = 0$ h) and $T = 3$ h, and multiplicity of growth calculated as cell counts at $T = 3$ h divided by cell counts at $T = 0$. The experiment to determine growth in human serum was exactly as described for the experiment to determine growth in blood, with the exception of the serum preparation. Briefly, the human blood was collected in collection vials with no additives, left to coagulate for 1 h at room temperature, and centrifuged at $1,500 \times g$ for 10 min, and the top layer (human serum) collected and used in the assay.

Mouse skin tissue histology and immunofluorescence staining. Skin and infected lesions excised from mice were fixed in 10% buffered formalin and submitted to the Translational Research Institute Histology Core Facility at The University of Queensland for processing and immunofluorescence staining. Briefly, the samples were processed in a Tissue-Tek VIP6 tissue processor and embedded with a Leica embedding station, which allows tissues to be oriented with the correct direction and then forms them into paraffin blocks. The tissue blocks were then sectioned at a 4-μm thickness and stained with hematoxylin and eosin (H&E) using Tissue-Tek Prisma and Glas for automated staining and coverslip addition. The histology slides were viewed and photographed under a Zeiss Axioplan 2 light microscope with a high-resolution Axiocam digital camera. We used the discovery ultra Ventana instrument (Roche) to perform immunofluorescence staining. The primary antibodies were used at a concentration of 1:100 to stain neutrophils (mouse anti-CD63 antibody; Abcam) and calprotectin (mouse anti-S100A9 antibody; Abcam) and a concentration of 1:300 to stain GAS (rabbit anti-group A carbohydrate antibody; Abnova). The secondary antibody was anti-mouse HQ antibody, supplied by Roche Ventana, followed by anti-HQ horseradish peroxidase (HRP) antibody, for 16 min each. The slides were stained with 3,3′-diaminobenzidine (DAB) and counterstained with hematoxylin (Hx).

Zinc measurements in skin tissue. Skin and infected-skin-lesion samples were excised from mice, weighed, and dissolved in 80% nitric acid at 80°C for 24 h. The samples were then diluted to 2% nitric acid and submitted for inductively coupled plasma mass spectrometry (ICP-MS) analysis at the School of Earth and Environmental Sciences, the University of Queensland. The final value was normalized to the weight of the skin tissue.

Human neutrophil killing assay. GAS survival following incubation with human neutrophils *in vitro* was assayed as previously described (11). To prevent phagocytosis, the neutrophil killing experiment was performed with the addition of cytochalasin D (Sigma). Briefly, the purified neutrophils were incubated with 10 μg/ml cytochalasin D for 15 min at 37°C and 5% CO_2 and then cooled on ice prior to the start of the experiment. Competition assays were performed with 50:50 WT/mutant mixtures, and bacterial survival was determined by enumerating colonies plated onto selective THY agar plates. The competitive index was a measure of total mutant colonies over total WT colonies.

Immunofluorescence microscopy and superresolution microscopy. Immunofluorescence microscopy was performed as previously described (11). The cells were stained with Alexa Fluor 488-conjugated rabbit anti-group A polysaccharide antibody (1:100 dilution, PAB13831; Abnova), Alexa Fluor 555-conjugated anti-LAMP1 antibody (1:100 dilution; Abcam), or anti-proteinase 3 antibody (1:100 dilution; Thermo Scientific) and Zinquin (25 μM; Sigma-Aldrich) for 3 h. For superresolution microscopy, cells were mounted on a no. 1.5-thickness coverslip using nonsolidifying mounting medium. The coverslips were then washed with Dulbecco's phosphate-buffered saline (DPBS) and mounted onto glass slides. Confocal images were acquired on a Zeiss LSM 510 metal confocal microscope (School of Chemistry and Molecular Biosciences, the University of Queensland), and superresolution images were acquired on a GE Healthcare OMX 3D-SIM superresolution microscope (Translational Research Institute Microscopy Core Facility at The University of Queensland).

Statistical analysis. Differences in relative gene expression, colony counts, lesion sizes, growth in human blood and serum, neutrophil survival, and competitive indices were analyzed using both the two-tailed unpaired *t* test and one-way analysis of variance (ANOVA) (GraphPad Prism). Differences in virulence were analyzed using the Mann-Whitney test (GraphPad Prism).

Ethics approval. All animal experiments were conducted according to the Guidelines for the Care and Use of Laboratory Animals (National Health and Medical Research Council, Australia) and were approved by the University of Queensland Animal Ethics Committee. Human blood donation for use in neutrophil killing and growth in blood and serum assays was conducted in accordance with the National Statement on Ethical Conduct in Human Research and in compliance with the regulations governing experimentation on humans and was approved by the University of Queensland Medical Research Ethics Committee.

SUPPLEMENTAL MATERIAL

Supplemental material for this article may be found at https://doi.org/10.1128/IAI.00048-18.

SUPPLEMENTAL FILE 1, PDF file, 1.5 MB.
SUPPLEMENTAL FILE 2, AVI file, 0.3 MB.
SUPPLEMENTAL FILE 3, AVI file, 0.2 MB.
SUPPLEMENTAL FILE 4, AVI file, 0.2 MB.
SUPPLEMENTAL FILE 5, AVI file, 0.2 MB.

ACKNOWLEDGMENTS

This research was supported by the National Health and Medical Research Council (NHMRC) via Australia Project grant number 1084460 and the Garnett Passe and Rodney Williams Memorial Foundation.

We thank the Translational Research Institute, Queensland, Australia, Histology Core Facility, and Crystal Chang for histology support. We thank the Translational Research Institute, Queensland, Australia, Microscopy Core Facility, and Sandrine Roy for superresolution microscopy support.

C.Y.O. performed all the experiments. O.B. assisted in constructing mutants and assisted with animal experiments. C.Y.O., A.G.M. and M.J.W. provided intellectual input and experimental design. C.Y.O., M.J.W. and A.G.M. wrote the manuscript. All authors reviewed and edited the manuscript.

The authors declare no competing interests.

REFERENCES

1. Waldron KJ, Robinson NJ. 2009. How do bacterial cells ensure that metalloproteins get the correct metal? Nat Rev Microbiol 7:25–35. https://doi.org/10.1038/nrmicro2057.
2. Djoko KY, Ong CL, Walker MJ, McEwan AG. 2015. The role of copper and zinc toxicity in innate immune defense against bacterial pathogens. J Biol Chem 290:18954–18961. https://doi.org/10.1074/jbc.R115.647099.
3. Kehl-Fie TE, Skaar EP. 2010. Nutritional immunity beyond iron: a role for

manganese and zinc. Curr Opin Chem Biol 14:218–224. https://doi.org/10.1016/j.cbpa.2009.11.008.
4. Zali H, Marashi SA, Rezaei-Tavirani M, Toossi P, Rahmati-Roodsari M, Shokrgozar MA. 2007. On the mechanism of apoptosis-inducing activity of human calprotectin: zinc sequestration, induction of a signaling pathway, or something else? Med Hypotheses 68:1012–1015. https://doi.org/10.1016/j.mehy.2006.09.056.
5. Corbin BD, Seeley EH, Raab A, Feldmann J, Miller MR, Torres VJ, Anderson KL, Dattilo BM, Dunman PM, Gerads R, Caprioli RM, Nacken W, Chazin WJ, Skaar EP. 2008. Metal chelation and inhibition of bacterial growth in tissue abscesses. Science 319:962–965. https://doi.org/10.1126/science.1152449.
6. Rahman MT, Karim MM. 2018. Metallothionein: a potential link in the regulation of zinc in nutritional immunity. Biol Trace Elem Res 182:1–13. https://doi.org/10.1007/s12011-017-1061-8.
7. Lichten LA, Cousins RJ. 2009. Mammalian zinc transporters: nutritional and physiologic regulation. Annu Rev Nutr 29:153–176. https://doi.org/10.1146/annurev-nutr-033009-083312.
8. Brophy MB, Hayden JA, Nolan EM. 2012. Calcium ion gradients modulate the zinc affinity and antibacterial activity of human calprotectin. J Am Chem Soc 134:18089–18100. https://doi.org/10.1021/ja307974e.
9. Makthal N, Nguyen K, Do H, Gavagan M, Chandrangsu P, Helmann JD, Olsen RJ, Kumaraswami M. 2017. A critical role of zinc importer AdcABC in group A streptococcus-host interactions during infection and its implications for vaccine development. EBioMedicine 21:131–141. https://doi.org/10.1016/j.ebiom.2017.05.030.
10. McDevitt CA, Ogunniyi AD, Valkov E, Lawrence MC, Kobe B, McEwan AG, Paton JC. 2011. A molecular mechanism for bacterial susceptibility to zinc. Plos Pathog 7:e1002357. https://doi.org/10.1371/journal.ppat.1002357.
11. Ong CLY, Gillen CM, Barnett TC, Walker MJ, McEwan AG. 2014. An antimicrobial role for zinc in innate immune defense against group A *Streptococcus*. J Infect Dis 209:1500–1508. https://doi.org/10.1093/infdis/jiu053.
12. Botella H, Peyron P, Levillain F, Poincloux R, Poquet Y, Brandli I, Wang C, Tailleux L, Tilleul S, Charriere GM, Waddell SJ, Foti M, Lugo-Villarino G, Gao Q, Maridonneau-Parini I, Butcher PD, Castagnoli PR, Gicquel B, de Chastellier C, Neyrolles O. 2011. Mycobacterial P-1-type ATPases mediate resistance to zinc poisoning in human macrophages. Cell Host Microbe 10:248–259. https://doi.org/10.1016/j.chom.2011.08.006.
13. Kapetanovic R, Bokil NJ, Achard ME, Ong CL, Peters KM, Stocks CJ, Phan MD, Monteleone M, Schroder K, Irvine KM, Saunders BM, Walker MJ, Stacey KJ, McEwan AG, Schembri MA, Sweet MJ. 2016. Salmonella employs multiple mechanisms to subvert the TLR-inducible zinc-mediated antimicrobial response of human macrophages. FASEB J 30:1901–1912. https://doi.org/10.1096/fj.201500061.
14. Ong CL, Walker MJ, McEwan AG. 2015. Zinc disrupts central carbon metabolism and capsule biosynthesis in *Streptococcus pyogenes*. Sci Rep 5:10799. https://doi.org/10.1038/srep10799.
15. Eijkelkamp BA, Morey JR, Ween MP, Ong CL, McEwan AG, Paton JC, McDevitt CA. 2014. Extracellular zinc competitively inhibits manganese uptake and compromises oxidative stress management in Streptococcus pneumoniae. PLoS One 9:e89427. https://doi.org/10.1371/journal.pone.0089427.
16. Walker MJ, Barnett TC, McArthur JD, Cole JN, Gillen CM, Henningham A, Sriprakash KS, Sanderson-Smith ML, Nizet V. 2014. Disease manifestations and pathogenic mechanisms of group A *Streptococcus*. Clin Microbiol Rev 27:264–301. https://doi.org/10.1128/CMR.00101-13.
17. Ferretti JJ, McShan WM, Ajdic D, Savic DJ, Savic G, Lyon K, Primeaux C, Sezate S, Suvorov AN, Kenton S, Lai HS, Lin SP, Qian YD, Jia HG, Najar FZ, Ren Q, Zhu H, Song L, White J, Yuan XL, Clifton SW, Roe BA, McLaughlin R. 2001. Complete genome sequence of an M1 strain of Streptococcus pyogenes. Proc Natl Acad Sci U S A 98:4658–4663. https://doi.org/10.1073/pnas.071559398.
18. Sanson M, Makthal N, Flores AR, Olsen RJ, Musser JM, Kumaraswami M. 2015. Adhesin competence repressor (AdcR) from Streptococcus pyogenes controls adaptive responses to zinc limitation and contributes to virulence. Nucleic Acids Res 43:418–432. https://doi.org/10.1093/nar/gku1304.
19. Weston BF, Brenot A, Caparon MG. 2009. The metal homeostasis protein, Lsp, of *Streptococcus pyogenes* is necessary for acquisition of zinc and virulence. Infect Immun 77:2840–2848. https://doi.org/10.1128/IAI.01299-08.
20. Tedde V, Rosini R, Galeotti CL. 2016. Zn2+ uptake in Streptococcus pyogenes: characterization of adcA and lmb null mutants. PLoS One 11:e0152835. https://doi.org/10.1371/journal.pone.0152835.
21. Linke C, Caradoc-Davies TT, Young PG, Proft T, Baker EN. 2009. The laminin-binding protein Lbp from Streptococcus pyogenes is a zinc receptor. J Bacteriol 191:5814–5823. https://doi.org/10.1128/JB.00485-09.
22. Plumptre CD, Eijkelkamp BA, Morey JR, Behr F, Counago RM, Ogunniyi AD, Kobe B, O'Mara ML, Paton JC, McDevitt CA. 2014. AdcA and AdcAII employ distinct zinc acquisition mechanisms and contribute additively to zinc homeostasis in Streptococcus pneumoniae. Mol Microbiol 91:834–851. https://doi.org/10.1111/mmi.12504.
23. Bayle L, Chimalapati S, Schoehn G, Brown J, Vernet T, Durmort C. 2011. Zinc uptake by Streptococcus pneumoniae depends on both AdcA and AdcAII and is essential for normal bacterial morphology and virulence. Mol Microbiol 82:904–916. https://doi.org/10.1111/j.1365-2958.2011.07862.x.
24. Aranda J, Garrido ME, Fittipaldi N, Cortes P, Llagostera M, Gottschalk M, Barbe J. 2010. The cation-uptake regulators AdcR and Fur are necessary for full virulence of Streptococcus suis. Vet Microbiol 144:246–249. https://doi.org/10.1016/j.vetmic.2009.12.037.
25. Le Breton Y, Mistry P, Valdes KM, Quigley J, Kumar N, Tettelin H, McIver KS. 2013. Genome-wide identification of genes required for fitness of group A Streptococcus in human blood. Infect Immun 81:862–875. https://doi.org/10.1128/IAI.00837-12.
26. Le Breton Y, Belew AT, Freiberg JA, Sundar GS, Islam E, Lieberman J, Shirtliff ME, Tettelin H, El-Sayed NM, McIver KS. 2017. Genome-wide discovery of novel M1T1 group A streptococcal determinants important for fitness and virulence during soft-tissue infection. Plos Pathog 13:e1006584. https://doi.org/10.1371/journal.ppat.1006584.
27. Prasad AS, Cossack ZT. 1982. Neutrophil zinc: an indicator of zinc status in man. Trans Assoc Am Phys 95:165–176.
28. Buchanan JT, Simpson AJ, Aziz RK, Liu GY, Kristian SA, Kotb M, Feramisco J, Nizet V. 2006. DNase expression allows the pathogen group A *Streptococcus* to escape killing in neutrophil extracellular traps. Curr Biol 16:396–400. https://doi.org/10.1016/j.cub.2005.12.039.
29. Andreini C, Bertini I, Cavallaro G, Holliday GL, Thornton JM. 2008. Metal ions in biological catalysis: from enzyme databases to general principles. J Biol Inorg Chem 13:1205–1218. https://doi.org/10.1007/s00775-008-0404-5.
30. Shankar AH., Prasad AS. 1998. Zinc and immune function: the biological basis of altered resistance to infection. Am J Clin Nutr 68:447S–463S. https://doi.org/10.1093/ajcn/68.2.447S.
31. Rink L, Gabriel P. 2000. Zinc and the immune system. Proc Nutr Soc 59:541–552. https://doi.org/10.1017/S0029665100000781.
32. Ibs KH, Rink L. 2003. Zinc-altered immune function. J Nutr 133:1452S–1456S. https://doi.org/10.1093/jn/133.5.1452S.
33. Wirth JJ, Fraker PJ, Kierszenbaum F. 1989. Zinc requirement for macrophage function: effect of zinc-deficiency on uptake and killing of a protozoan parasite. Immunology 68:114–119.
34. James SJ, Swendseid M, Makinodan T. 1987. Macrophage-mediated depression of T-cell proliferation in zinc-deficient mice. J Nutr 117:1982–1988. https://doi.org/10.1093/jn/117.11.1982.
35. Karl L, Chvapil M, Zukoski CF. 1973. Effect of zinc on viability and phagocytic capacity of peritoneal macrophages. Proc Soc Exp Biol Med 142:1123–1127. https://doi.org/10.3181/00379727-142-37190.
36. Chvapil M, Stankova L, Bernhard DS, Weldy PL, Carlson EC, Campbell JB. 1977. Effect of zinc on peritoneal macrophages in vitro. Infect Immun 16:367–373.
37. Andreini C, Banci L, Bertini I, Rosato A. 2006. Zinc through the three domains of life. J Proteome Res 5:3173–3178. https://doi.org/10.1021/pr0603699.
38. Elsner A, Kreikemeyer B, Braun-Kiewnick A, Spellerberg B, Buttaro BA, Podbielski A. 2002. Involvement of Lsp, a member of the Lral-lipoprotein family in Streptococcus pyogenes, in eukaryotic cell adhesion and internalization. Infect Immun 70:4859–4869. https://doi.org/10.1128/IAI.70.9.4859-4869.2002.
39. Brenot A, Weston BF, Caparon MG. 2007. A PerR-regulated metal transporter (PmtA) is an interface between oxidative stress and metal homeostasis in *Streptococcus pyogenes*. Mol Microbiol 63:1185–1196. https://doi.org/10.1111/j.1365-2958.2006.05577.x.
40. Tenenbaum T, Spellerberg B, Adam R, Vogel M, Kim KS, Schroten H. 2007. Streptococcus agalactiae invasion of human brain microvascular endothelial cells is promoted by the laminin-binding protein Lmb. Microbes Infect 9:714–720. https://doi.org/10.1016/j.micinf.2007.02.015.

41. Brinkmann V, Reichard U, Goosmann C, Fauler B, Uhlemann Y, Weiss DS, Weinrauch Y, Zychlinsky A. 2004. Neutrophil extracellular traps kill bacteria. Science 303:1532–1535. https://doi.org/10.1126/science.1092385.
42. Urban CF, Ermert D, Schmid M, Abu-Abed U, Goosmann C, Nacken W, Brinkmann V, Jungblut PR, Zychlinsky A. 2009. Neutrophil extracellular traps contain calprotectin, a cytosolic protein complex involved in host defense against Candida albicans. Plos Pathog 5:e1000639. https://doi.org/10.1371/journal.ppat.1000639.
43. Teigelkamp S, Bhardwaj RS, Roth J, Meinardus-Hager G, Karas M, Sorg C. 1991. Calcium-dependent complex assembly of the myeloic differentiation proteins MRP-8 and MRP-14. J Biol Chem 266:13462–13467.
44. Fagerhol MK, Dale I, Andersson T. 1980. A radioimmunoassay for a granulocyte protein as a marker in studies on the turnover of such cells. Bull Eur Physiopathol Respir 16(Suppl):273–282.
45. Johne B, Fagerhol MK, Lyberg T, Prydz H, Brandtzaeg P, Naess-Andresen CF, Dale I. 1997. Functional and clinical aspects of the myelomonocyte protein calprotectin. Mol Pathol 50:113–123. https://doi.org/10.1136/mp.50.3.113.
46. Huang L, Tepaamorndech S. 2013. The SLC30 family of zinc transporters: a review of current understanding of their biological and pathophysiological roles. Mol Aspects Med 34:548–560. https://doi.org/10.1016/j.mam.2012.05.008.
47. Jeong J, Eide DJ. 2013. The SLC39 family of zinc transporters. Mol Aspects Med 34:612–619. https://doi.org/10.1016/j.mam.2012.05.011.
48. Taylor CM, Goode HF, Aggett PJ, Bremner I, Walker BE, Kelleher J. 1992. Symptomatic zinc deficiency in experimental zinc deprivation. J Clin Pathol 45:83–84. https://doi.org/10.1136/jcp.45.1.83.
49. Hennigar SR, Kelleher SL. 2015. TNFalpha post-translationally targets ZnT2 to accumulate zinc in lysosomes. J Cell Physiol 230:2345–2350. https://doi.org/10.1002/jcp.24992.
50. Chatellier S, Ihendyane N, Kansal RG, Khambaty F, Basma H, Norrby-Teglund A, Low DE, McGeer A, Kotb M. 2000. Genetic relatedness and superantigen expression in group A *Streptococcus* serotype MZ isolates from patients with severe and nonsevere invasive diseases. Infect Immun 68:3523–3534. https://doi.org/10.1128/IAI.68.6.3523-3534.2000.
51. Wertman KF, Wyman AR, Botstein D. 1986. Host vector interactions which affect the viability of recombinant phage lambda clones. Gene 49:253–262. https://doi.org/10.1016/0378-1119(86)90286-6.
52. Zhang X, Ding L, Sandford AJ. 2005. Selection of reference genes for gene expression studies in human neutrophils by real-time PCR. BMC Mol Biol 6:4. https://doi.org/10.1186/1471-2199-6-4.
53. Leung KW, Liu MG, Xu XM, Seiler MJ, Barnstable CJ, Tombran-Tink J. 2008. Expression of ZnT and ZIP zinc transporters in the human RPE and their regulation by neurotrophic factors. Invest Ophthalmol Vis Sci 49:1221–1231. https://doi.org/10.1167/iovs.07-0781.
54. Sun HM, Ringdahl U, Homeister JW, Fay WP, Engleberg NC, Yang AY, Rozek LS, Wang XX, Sjobring U, Ginsburg D. 2004. Plasminogen is a critical host pathogenicity factor for group A streptococcal infection. Science 305:1283–1286. https://doi.org/10.1126/science.1101245.